Crack opening estimate in reinforced concrete walls using a steel–concrete bond model

Chetra Mang, Ludovic Jason, Luc Davenne

Chetra Mang, Ludovic Jason, Luc Davenne. Crack opening estimate in reinforced concrete walls using a steel–concrete bond model. Archives of civil and mechanical engineering, 2016, 16 (3), pp.422--436. ⟨10.1016/j.acme.2016.02.001⟩. ⟨hal-01411074⟩

Crack opening estimate in reinforced concrete walls using a steel-concrete bond model

C. Mang[a,c], L. Jason[a,b,*], L. Davenne[c]

[a] SEMT, CEA DEN, Université Paris Saclay, 91191 Gif sur Yvette Cedex, France

[b] IMSIA, CEA, CNRS, EDF, ENSTA Paristech, Université Paris Saclay, 91762 Palaiseau Cedex, France

[c] LEME, Université Paris Ouest, F-92410 Ville d'Avray, France

Corresponding author :

Ludovic Jason

Atomic Energy Commission (CEA), Mechanics and System Simulation Laboratory (LM2S)

Email address: ludovic.jason@cea.fr,

Crack opening estimate in reinforced concrete walls using a steel-concrete bond model

Abstract

This paper presents the application of a new steel-concrete bond model on a reinforced concrete shear wall, experimentally tested during the French National Project CEOS.FR. The proposed results include both global (evolution of the force as a function of the displacement for example) and local results (crack opening and spacing). A new post-processing method to compute these local properties even in a case of a complex crack pattern (oriented cracks for example) is proposed. It is based on the change in the sign of the bond slip between steel and concrete. The simulated results are in a good agreement with the experiment and validate the developments. Finally, the interest of including a specific steel-concrete bond model in the finite element simulation is highlighted, compared to classical "no-slip" relation.

Keyword: reinforced concrete, crack spacing, crack opening, steel-concrete bond, shear wall

1 Introduction

In particular cases, the estimation of the crack properties (spacing and opening especially) is a key point in the design and the evaluation of reinforced concrete structures ([1],[2]). Cracking may indeed question the safety and the durability (loss of confinement, corrosion of rebars or leakage issue for example). Development of cracks in reinforced concrete structures is a complex phenomenon. It includes crack initiation, propagation, change from microcracks to macrocracks and interactions between concrete and reinforcement [3]. Among the different available approaches (discrete approach [4], cohesive zones [5], …), damage models are widely used in literature to describe the initiation and propagation of cracks. Based on continuum mechanics, they include a reduction in the stiffness [6] and may be associated to irreversible strains ([7], [8]), crack closure or to an isotropic or orthotropic description of the mechanical degradation ([9], [10]).

In this context, when large reinforced concrete structures are considered, a no-slip (also called "perfect") relation is generally assumed to model the steel-concrete interface. But this hypothesis may have heavy consequences when the crack properties are studied, as the steel – concrete bond directly influences their evolutions. For example, in [1], an engineering law is provided which directly relates the crack spacing and the bond properties. In [11], bond effect is underlined and is responsible for a different cracking behavior, compared to classical perfect relation, especially in the active cracking phase (for bending reinforced concrete beams).

To solve this problem, numerical models have been developed to represent the steel – concrete bond more accurately. For example, Ngo and Scordelis [12] proposed a spring element to relate concrete and steel nodes, associated to a linear constitutive law. An interface element in 2D was then introduced by Brancherie and Ibrahimbegovic [13] or Dominguez et al. [14] which enables the use of a nonlinear law. Dominguez [15] and Ibrahimbegovic et al. [16] among others finally proposed an embedded element in which the bond behavior is described through an enrichment of the degrees of freedom. Even if these approaches lead to a correct description of the bond mechanisms between steel and concrete, they also have their own limits, especially in cases of real scale

applications: meshing problems (explicit representation of 3D steel geometry) or increase in computation time (with enriched elements). That is why alternative solutions were proposed [17] to represent the effects of the steel-concrete bond in a context adapted to large scale applications: truss steel elements are used for reinforcement with no need to explicitly mesh the steel-concrete interface.

The latter was improved in [21] and applied on a reinforced concrete tie. Even if the results were promising (capacity of the model to reproduce the global and local experimental results), they were limited to simplified uniaxial loading. For more complex situations, especially in the case of more complex crack patterns, the results were questionable. This paper proposes to evaluate the performance of the model on a reinforced concrete shear wall. In the first part, the steel-concrete bond model is briefly recalled. In the second part, the test case is presented, associated to the results concerning the global behavior. Due to the use of a damage model for concrete, a new post-processing method, based on the slip between steel and concrete, is proposed to calculate the crack properties. This method is applied on the shear wall and a comparison with the experiment is performed. Finally, a discussion is proposed to evaluate the interest of the steel-concrete bond model compared to a "perfect" no-slip relation.

2 Description of the bond slip model

When reinforced concrete structures are considered, one of the most classical hypotheses is to model the steel reinforcement as truss (or membrane) elements and to consider a perfect relation between steel and concrete. This perfect relation is generally applied through kinematic relations between both models, using the shape functions of each element. But this hypothesis may have heavy consequences, especially when the crack properties (spacing and openings) are studied, as the steel – concrete bond directly influences their evolutions ([1], [11] for example). To take into account this interfacial behavior between steel and concrete in a more appropriate manner, the new interface element developed in [21], based on the previous work from Casanova et al [17], is used. It is a zero thickness four node element which relates each steel truss element with an associated superimposed segment, perfectly bonded to the surrounding concrete (Figure 1).

Each node of the interface element has three degrees of freedom (nodal displacements) (Figure 2). The relation between the generalized slip in the local direct frame $\{\delta(p)\}$ (Figure 3) and the nodal displacements $\{u\}$ is written in the following form:

$$\{\delta(p)\} = \left\{\delta_t(p) \quad \delta_{n_1}(p) \quad \delta_{n_2}(p)\right\}^T = \overline{\overline{B}}(p)\{u\} \tag{1}$$

with

$$\overline{\overline{B}}(p) = \left[\overline{\overline{B_1}}(p) \quad \overline{\overline{B_2}}(p) \quad -\overline{\overline{B_1}}(p) \quad -\overline{\overline{B_2}}(p)\right] \tag{2}$$

and

$$\begin{aligned} \overline{\overline{B_1}}(p) &= 0.5(1-p)\overline{\overline{I_3}} \\ \overline{\overline{B_2}}(p) &= 0.5(1+p)\overline{\overline{I_3}} \end{aligned} \tag{3}$$

where $\overline{\overline{I_3}} = \begin{bmatrix} 1 & 0 & 0 \\ 0 & 1 & 0 \\ 0 & 0 & 1 \end{bmatrix}$ and $-1 \le p \le 1$ (Figure 3).

Constitutive laws are defined between the bond stress $\{\sigma(p)\} = \begin{Bmatrix} \sigma_t(p) \\ \sigma_{n_1}(p) \\ \sigma_{n_2}(p) \end{Bmatrix}$ and the bond slip $\{\delta(p)\}$.

In the tangential direction, the tangential stress σ_t is computed from the tangential slip:

$$\sigma_t(p) = f(\delta_t(p)) \quad (4)$$

In this contribution, the bond law follows the recommendations from Torre-Casanova et al [19], especially for the definition of the maximum bond stress $\sigma_{t,max}$ (Figure 4):

$$\frac{\sigma_{t,\max}}{f_t} = 1.53\frac{c}{d_s} + 0.36 \quad \text{if} \quad \frac{c}{d_s} < \left(\frac{c}{d_s}\right)_{spl-pul} \quad (5)$$

$$\frac{\sigma_{t,\max}}{f_c} = 0.6 \quad \text{if} \quad \frac{c}{d_s} \ge \left(\frac{c}{d_s}\right)_{spl-pul} \quad (6)$$

with f_t and f_c respectively the tensile and compressive concrete strengths, c the concrete cover and d_s the steel diameter.

$$\left(\frac{c}{d_s}\right)_{spl-pul} = 0.39\frac{f_c}{f_t} - 0.24 \quad (7)$$

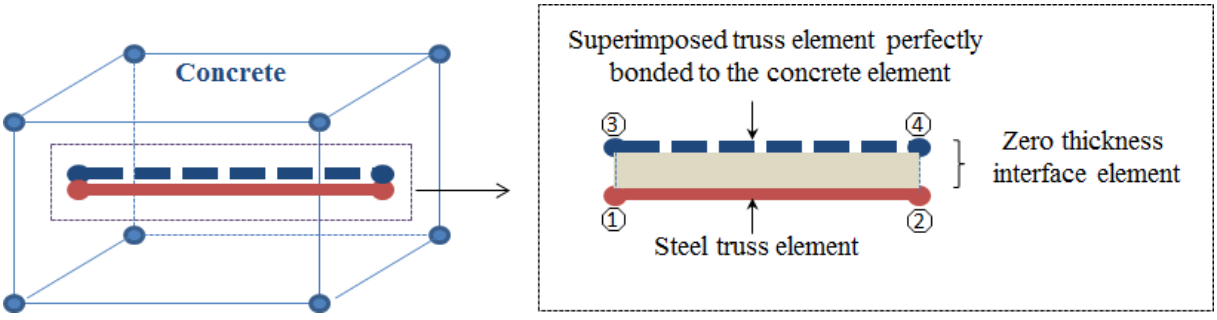

Figure 1. Principle of the interface element between steel and concrete [18]

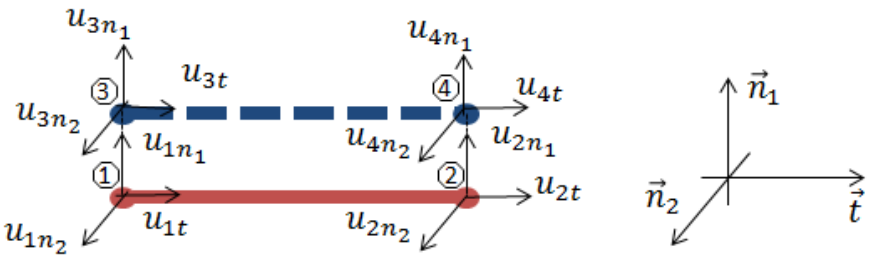

Figure 2. Degrees of freedom of the interface element [18]

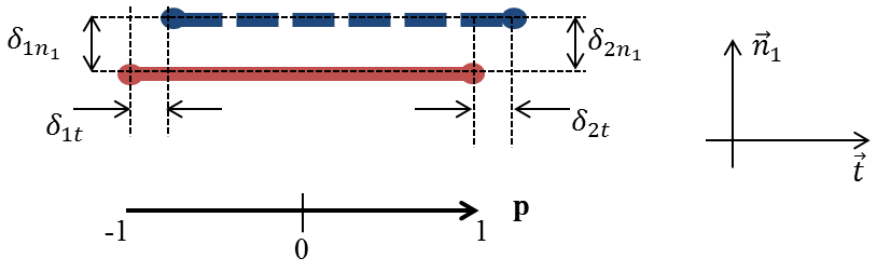

Figure 3. Definition of the slip between steel and concrete in the interface element in the ($\vec{t}$, $\vec{n_1}$) plane [18]

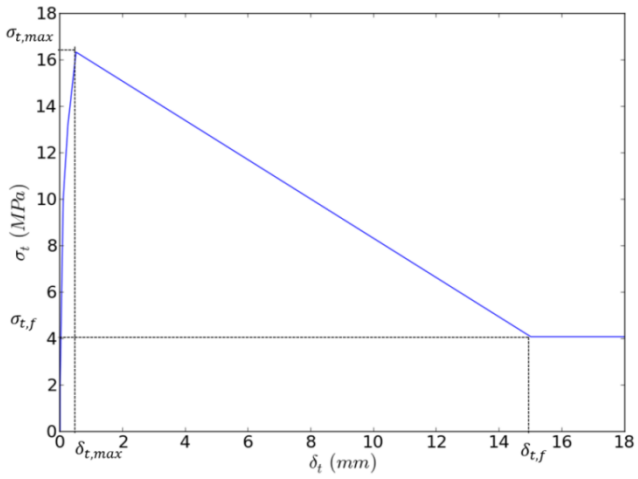

Figure 4. Example of a bond law in the tangential direction

In the normal directions, for sake of simplicity, a linear relation is assumed between the stresses σ_{n1} and σ_{n2} and the corresponding normal slips:

$$\begin{Bmatrix} \sigma_{n_1}(p) \\ \sigma_{n_2}(p) \end{Bmatrix} = k_n \begin{Bmatrix} \delta_{n_1}(p) \\ \delta_{n_2}(p) \end{Bmatrix} \quad (8)$$

The value of the normal stiffness is chosen high enough to be representative of a perfect bond (k_n = 10^{15} Pa.m^{-1} in the following). Additional information can be found in [18].

3 Application to a reinforced concrete shear wall

The developed model is applied to a reinforced concrete shear wall tested during the French National Project CEOS.FR [20].

1.1. Description of the shear wall

The dimensions of the current part of the shear wall are 4.2m x 1.05m x 0.15m (Figure 5). The reinforcement is performed using a double steel frame (10 mm diameter) with a 100 mm space in both vertical and horizontal directions (concrete cover equal to 10 mm). To prevent the crack opening due to bending, additional reinforcement is added at each extremity of the wall (25 and 32 mm bars). Two horizontal high strength concrete beams are connected to upper and bottom parts of the wall to ensure a correct distribution of the shear force [21]. An increasing horizontal displacement is applied on the top of the wall through one jack (center of the jack located at a height of 1.85 m from the bottom of the experimental device) [22]. Four prestressed bars are used in the lower concrete beams to relate the structure to the ground.

Several sensors were deployed to control the test and monitor the structural and cracking behavior. Especially, cracking pattern is achieved by applying a Digital Image correlation technique together with a post-processing algorithm for cracks detection and measuring [30].

Figure 5. Shear wall experimental setup [22]

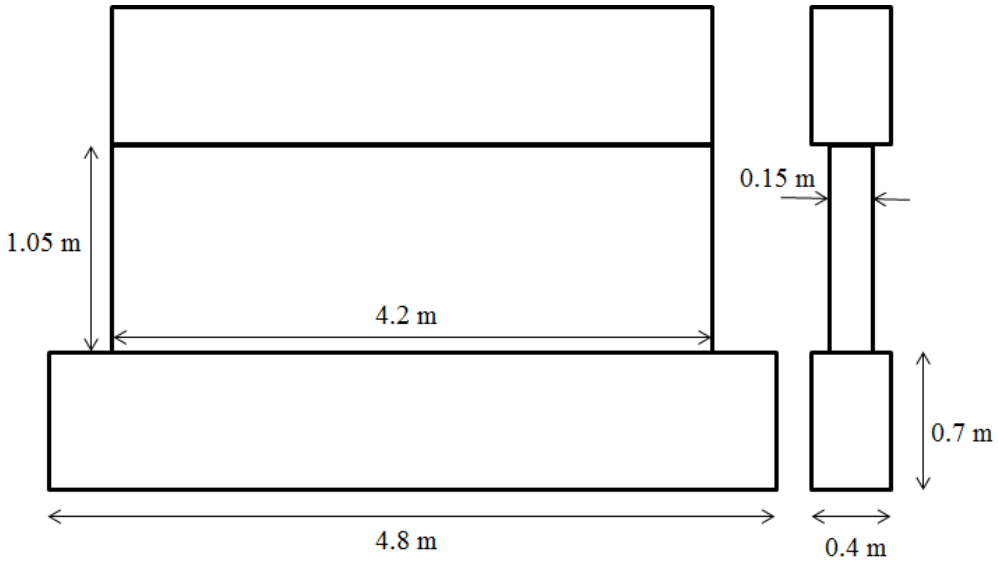

Figure 6. Dimensions of the shear wall

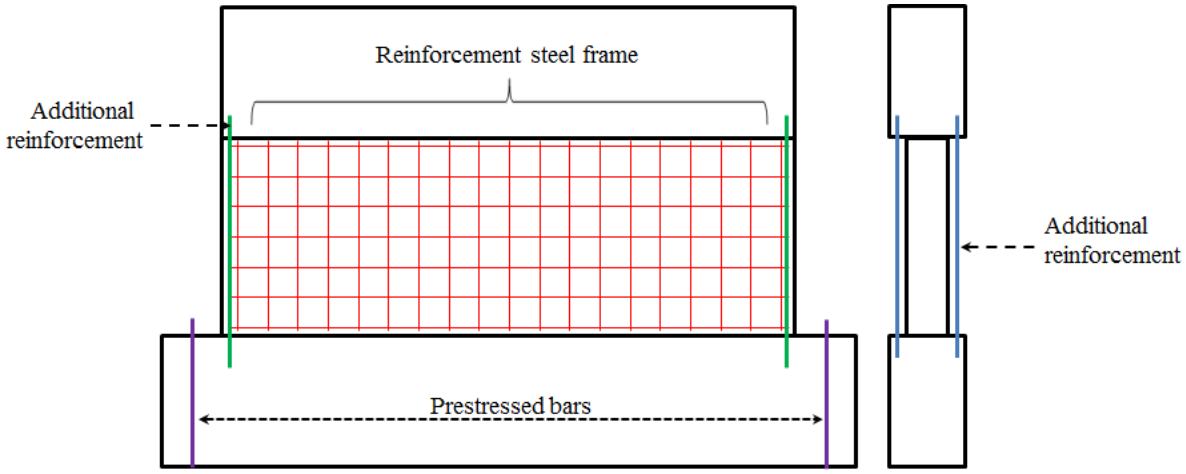

Figure 7. Reinforcement in the shear wall

A 3D simulation is performed with the finite element code Cast3M [23] using solid elements for concrete (40 mm x 40 mm x 37.5 mm mesh) and truss elements for reinforcements (main and additional reinforcements) (Figure 8). Steel is modeled using an elastic plastic model with linear hardening. The associated parameters, experimentally measured, are listed in Table 1. Concrete, in its central part, is represented using a damage constitutive law developed in [7]. This law was chosen because it was successfully applied in previous works [11]. Damage is represented by two independent variables d^+ and d^- which have respectively an influence in tension and compression. The stress σ is evaluated using the following relation:

$$\sigma = \left[1 - d^+\left(\sigma'^+\right)\right]\sigma'^+ + \left[1 - d^-\left(\sigma'^-\right)\right]\sigma'^- \quad (9)$$

where σ'^+ and σ'^- correspond respectively to the positive and the negative parts of the effective stress σ':

$$\sigma' = C\left(\varepsilon - \varepsilon^p\right) \quad (10)$$

In this relation, *C* is the tensor of elasticity and *ε* represents the total strain. ε^p symbolizes the irreversible strains governed by the damage evolution in compression.

$$\dot{\varepsilon}^p = \beta E H(\dot{d}^-)\frac{\langle \sigma' : \dot{\varepsilon} \rangle}{\sigma' : \sigma'} C^{-1} : \sigma' \quad (11)$$

where β is a model parameter, *E* the Young modulus and *H* the Heaviside function. $\langle . \rangle$ represents the positive part of the tensor. The tensile part of the model is regularized using a Hillerborg technique that guarantees a constant energy release independent on the mesh size [3].

The model parameters have been chosen to be as representative as possible to the experimental properties given in Table 2. Top and bottom beams are considered elastic during the simulation. For the bond model, a piecewise linear curve is chosen for the evolution *f* of the bond slip as a function of the bond stress (equation (4)), following the recommendations from [19]. Especially, the maximum bond strength is computed using the equations:

$$\left(\frac{c}{d_s}\right)_{spl-pul} = 0.39\frac{f_c}{f_t} - 0.24 = 0.39\frac{42.5}{3.3} - 0.24 = 4.78 \quad (12)$$

As $\left(\frac{c}{d_s}\right) = \frac{0.01}{0.01} = 1$ is less than $\left(\frac{c}{d_s}\right)_{spl-pul}$,

$$\sigma_{t,\max} = f_t(1.53\frac{c}{d_s} + 0.36) = 6.24 \text{ MPa} \quad (13)$$

The resulting parameters are given in Table 3 and the associated curve in Figure 9.

An increasing horizontal displacement u_x is applied to the wall (Figure 10). A vertical force *p* (520 kN) is applied on each prestressed bar. A zero horizontal displacement is also imposed on the right extremity of the bottom beam as in the experiment.

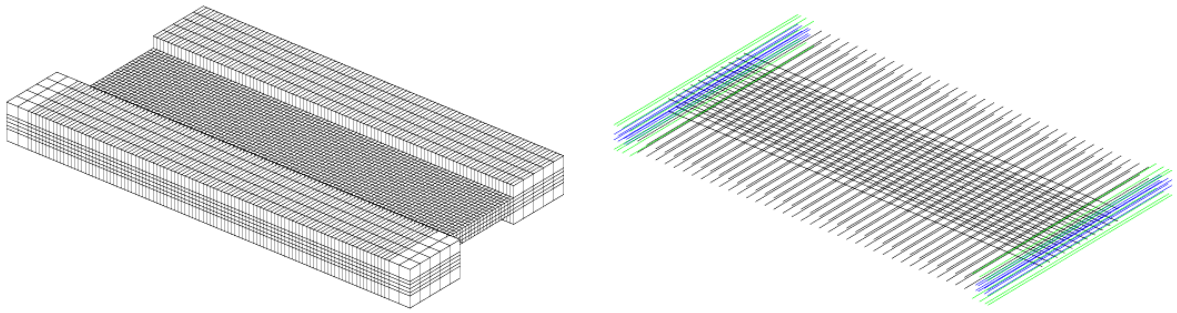

Figure 8. Concrete (left) and steel (right) meshes.

Young modulus	Poisson ratio	Limit of elasticity	Hardening modulus
E_s (GPa)	ν_s	σ_s^e (MPa)	E_h (MPa)
190	0.3	554	3245

Table 1. Measured steel properties

Young modulus	Poisson ratio	Tensile strength	Compressive strength
E_c (GPa)	ν_c	f_t (MPa)	f_c (MPa)
22	0.19	3.3	42.5

Table 2. Experimentally obtained concrete parameters [22]

Bond stress (MPa)	2	6,2	2	2
Bond slip (mm)	0,02	0,17	15	16
Slope (Pa.m^{-1})	10^{12}	2,5 10^{10}	-2,9 10^{8}	0

Table 3. Parameters of the bond slip – bond stress law

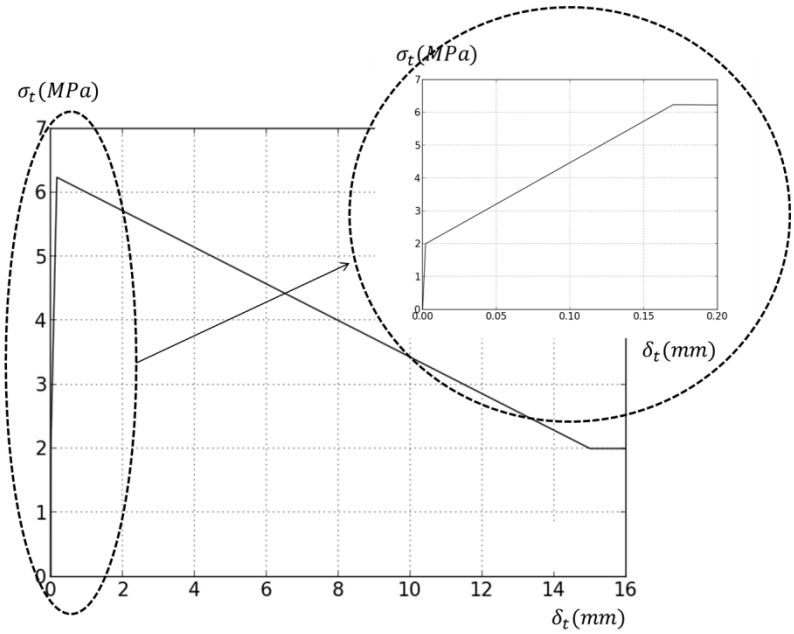

Figure 9. Bond slip – bond stress law

Figure 10. Loading and boundary conditions

3.1 Results

3.1.1 Global behavior

Figure 11 illustrates the evolution of the applied force as a function of the relative displacement (difference in the horizontal displacement between top and bottom parts of the wall). The experimental behavior, obtained from classical displacement sensors located on the top and bottom points of the external face at mid-length, is well reproduced by the simulation with especially a correct value of the maximum applied force before failure. It is to be noted that the elastic part does not seem to be totally satisfactory compared to the displacement sensor measurement. To check the elastic evolution, the relative displacements provided by digital image correlation (Figure 11 right) are used. In this case, the simulated elastic evolution is correct. The difference between simulation and experiment on Figure 11 left seems thus to come from an experimental difficulty, also reported in [21]. As a conclusion, the finite element simulation is able to represent the main characteristics of the global behavior.

3.1.2 Damage evolution

The most direct result concerning the mechanical degradation, when using a damage model, is the damage distribution. Figure 12 compares the damage distributions with the crack patterns experimentally observed on the external face for different level of loading.

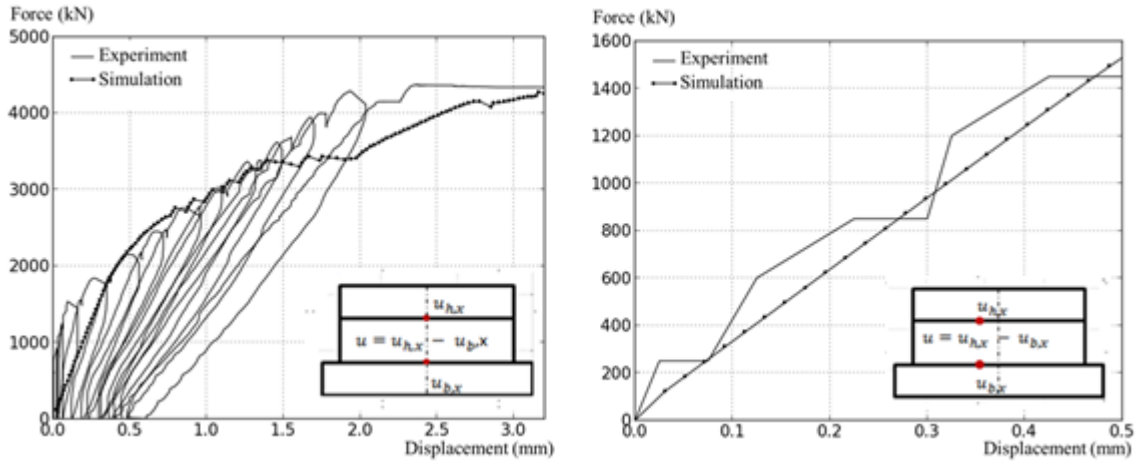

Figure 11. Force-displacement curve from displacement sensor (left) and digital image correlation (right).

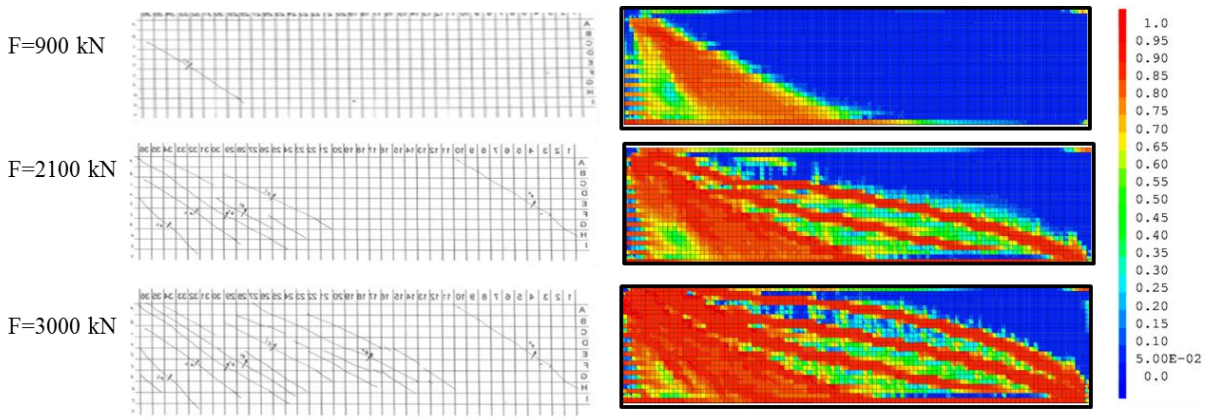

Figure 12. Evolution of the damage distribution (right) and comparison with the experimental crack patterns (left). Red zones are the most damaged ones.

A good qualitative agreement is obtained. Nevertheless, it is not possible to obtain direct information concerning the position and the opening of the cracks. That is why, in the next part of the paper, a new post-processing method is described to compute the crack properties.

4 A new method to compute crack spacing and opening

If damage models generally succeed in reproducing the consequences of the crack initiation and propagation even up to failure, they fail in representing explicitly the crack characteristics as they are, by definition, based on a continuous description of the problem. To overcome this difficulty, different solutions exist. Combined approaches ([24], [25], [26]) take advantage of the damage model to describe the crack initiation and combine them with more adapted techniques once cracks propagate. In [27], the strong discontinuity approach is proposed to relate classical fracture mechanics properties to the continuum model properties. In [24], an isotropic regularized model is chosen until the damage band reaches a given value. From this point, equivalence with XFeM method is proposed to represent the crack and their propagation. The key point of these methods is generally the criterion from which both methods communicate.

Post-processing methods represent another, and probably simpler, alternative. They are based on the analysis of the results after the end of the simulation. For example, Dufour et al [28] propose to reanalyze the results from an analytical strain field obtained with the strong discontinuity approach. Matallah et al [29] define a cracking strain and an equivalent length from which the crack opening is computed. In this paper, a new method is proposed, which takes directly advantage of the use of a steel – concrete bond model and of the calculation of the steel-concrete slip. The proposed method can be used independently on the considered damage models as it only uses the distribution of the slip along the interface.

4.1 Determination of the crack spacing

4.1.1 New method based on the steel-concrete slip

The proposed method takes directly advantage of the developed bond model presented in the previous section. It is based on the fact that the crack position corresponds to a change in the sign of the bond slip (Figure 13). The slips along the steel bars are then computed to locate the changes in the sign. These points correspond to the position of the crack.

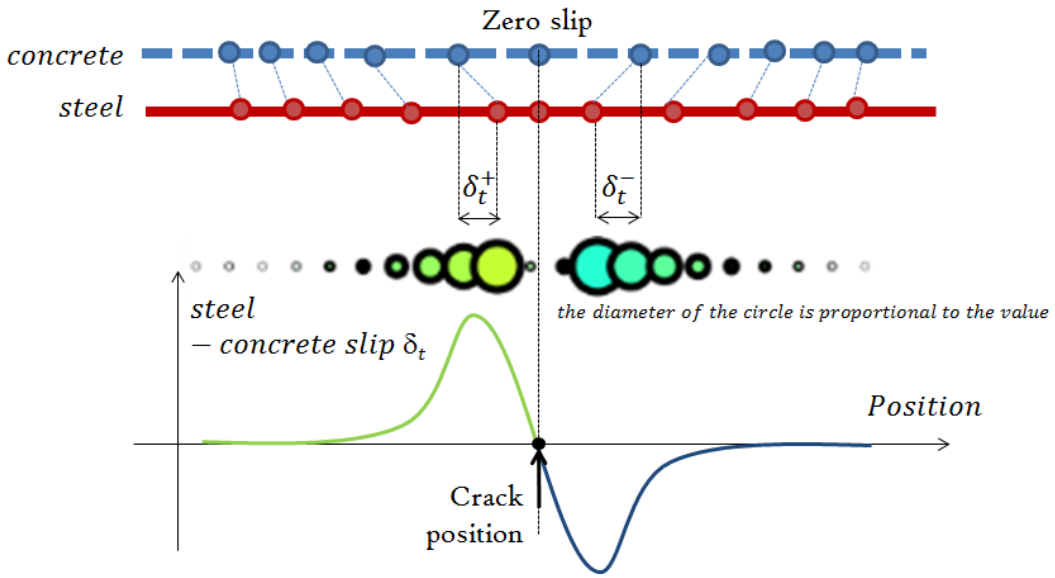

Figure 13. Definition of the change in the sign of the tangential slip

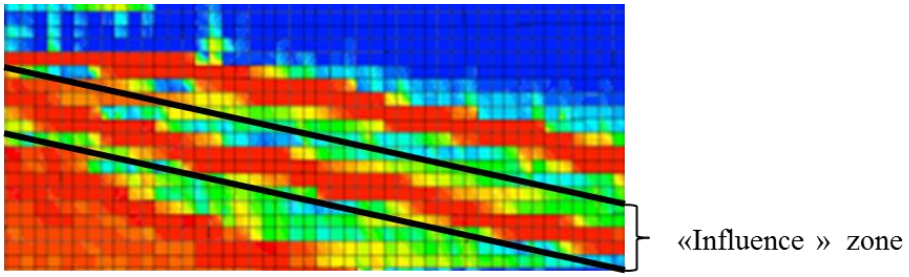

Figure 14. Example of the definition of the « influence » zone from the damage distribution

From these positions, the crack path, at the reinforcement, is determined by relating each point of a crack in its “influence” zone. This influence zone is only used to distinguish one crack to another. In this sense, it can be defined in an intuitive way (from the distribution of the mechanical damage for example to evaluate the fracture process zone related to each crack - Figure 14). It is the case in our contribution in which “by-hand” influence zones are defined where a given crack is expected to be located. Some automatic criteria could also be used to define the crack path from one point to another (limited evolution of the angle of the cracks from one point to the following for example, definition of a search direction determined by the two previous points in the crack path [28]).

As this method uses the slip between steel and concrete, it is to be noted that the crack path is computed at the position of the reinforcements. If other locations are needed (external faces for example), a hypothesis is needed to interpolate the crack paths in the cross section. In our case, crossing cracks are considered and each crack path is supposed to be the same in the depth of the wall. This hypothesis can be checked from a comparison between the crack positions at the inner and outer reinforcement layers and from a comparison at the external face of the structure, using the alternative post-processing method which is presented in the following section.

4.1.2 Alternative method based on the displacement steps

When slip is not available (perfect no-slip hypothesis for example) or to check crossing crack hypothesis, an alternative solution must be defined to compute the crack spacing. A more classical

approach based on the displacement steps on the external face is thus proposed. It supposes (Figure 15 and Figure 16):

- the computation of the displacement step between two neighboring points (called "1" and "2" in the following) $\Delta\vec{u} = \vec{u_2} - \vec{u_1}$ and of the norm $\left\|\Delta\vec{u}\right\|$ ($\left\|\Delta\vec{u}\right\| = \sqrt{\Delta u_x^2 + \Delta u_y^2}$). The displacements are computed directly from the nodal displacements. This method imposes to choose, a priori, a post-processing direction for the calculation of the difference in the displacements, which may not be coincident with the crack direction. In our cases, the horizontal direction is chosen.
- the definition of the crack position from the local maximum of $\left\|\Delta\vec{u}\right\|$ along each horizontal line (using the same post-processing direction). An arbitrary criterion, w_c, is used to eliminate the noise ($\left\|\Delta\vec{u}\right\| < w_c$).
- the definition of the crack path from one point to another using the same method as previously described

This method, closer to the experimental method developed for digital correlation ([30] or [31]) has two main drawbacks. First, some cracks may be forgotten if the post processing direction is too far from the crack direction (for example, if the horizontal direction is chosen, vertical cracks cannot be detected) or several post-processing must be done using different post-processing directions.

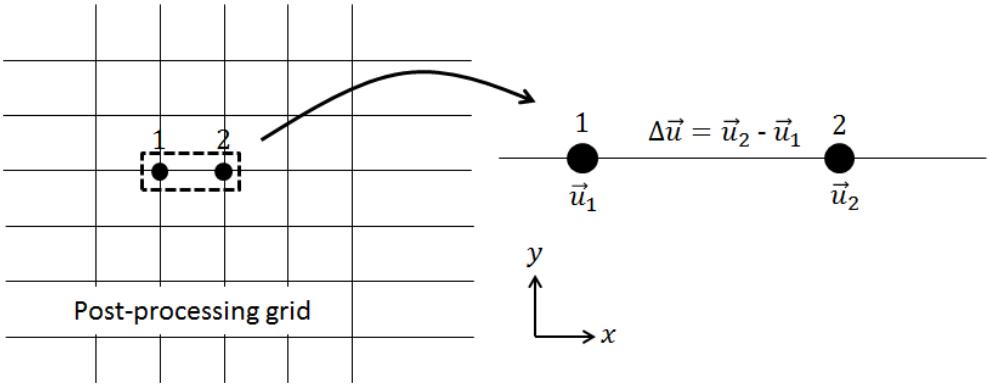

Figure 15. Calculation of the relative displacements

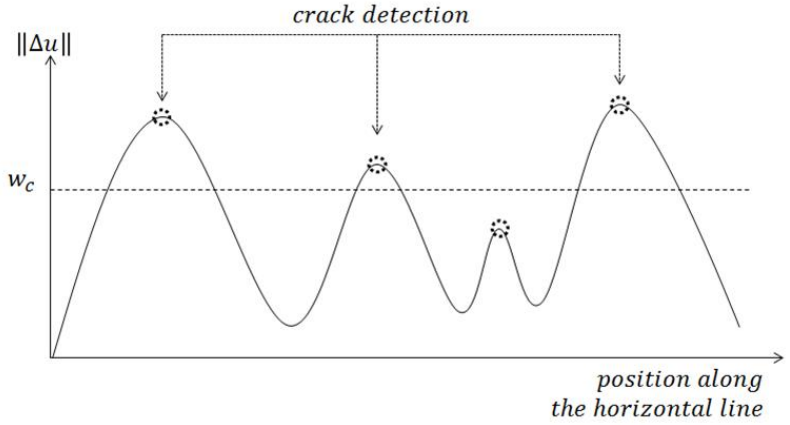

Figure 16. Principle of the « crack » detection

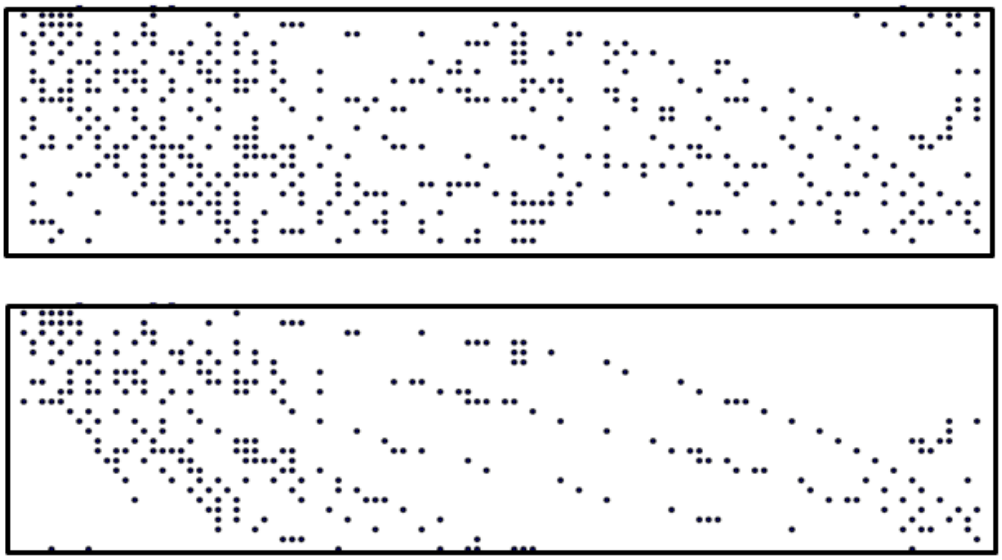

Figure 17. Example of the crack position obtained from the relative displacements on the external face with two different values of w_c (top : 20 µm, bottom 100 µm)

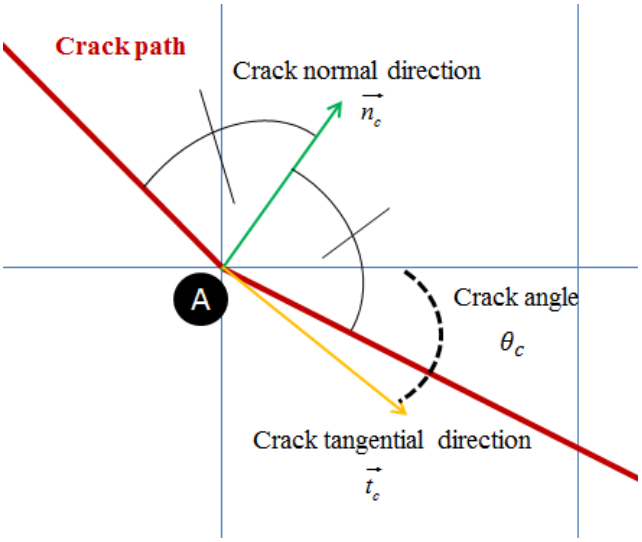

Figure 18. Definition of the crack normal direction

Moreover, the results may be dependent on the choice for w_c (Figure 17). In this sense, the method based on the change in the slip sign represents a suitable alternative as it does not suppose any hypothesis for the crack detection.

4.2 Crack opening

The crack opening is here defined as the opening in the normal direction of the crack. At each point of the previously defined crack path, the normal and tangential crack directions ($\vec{n_c}$ and $\vec{t_c}$ respectively) and the crack angle θ_c are determined (Figure 18). The normal direction is defined from the bisector of the two adjacent segments of the crack path and thus evolves along the crack path. The tangential direction is calculated to obtain a direct reference frame.

The crack opening is then computed from the relative displacement in the normal direction at the crack position. The methodology supposes the following steps for each crack point (Figure 19):

- definition of a post-processing line in the normal crack direction. The line is chosen long enough to include the potential effect of regularization in the neighborhood of the crack. In our example, this length is taken equal to the half-spacing between calculated cracks in the normal direction
- discretization of the post-processing line in post-processing points at which the normal relative displacement is computed.
- computation of the relative displacement in the normal direction Δu_n along the post processing line using the shape functions of the finite elements if necessary.
- sum of the computed relative displacements along the post-processing line to obtain the normal crack opening w ($w = \sum_{\text{post-processing line}} \Delta u_n$)

Compared to [29] or [32], the calculation of the crack opening does not imply the definition of an element length, as it is directly based on the displacements and not on the strains. The length of the post-processing line can be related to a "physical" parameter (half-spacing for example). Moreover, it is applicable even in the case of a regularized computation ([33] for example) in which the strains are not fully localized.

5 Crack calculation on the shear wall

5.1 Crack spacing

The proposed method based on the change in the slip sign is applied on the shear wall. The bond slip along the reinforcement frame is calculated (Figure 20) and the change in the sign is localized (Figure 21). The crack path is then determined. To compare with the experimental results using the digital image correlation, information are needed on the external face. The simulated cracks are assumed to cross the wall with identical positions at the steel-concrete interface and on the external face. This hypothesis is checked using the alternative method based on the displacements steps.

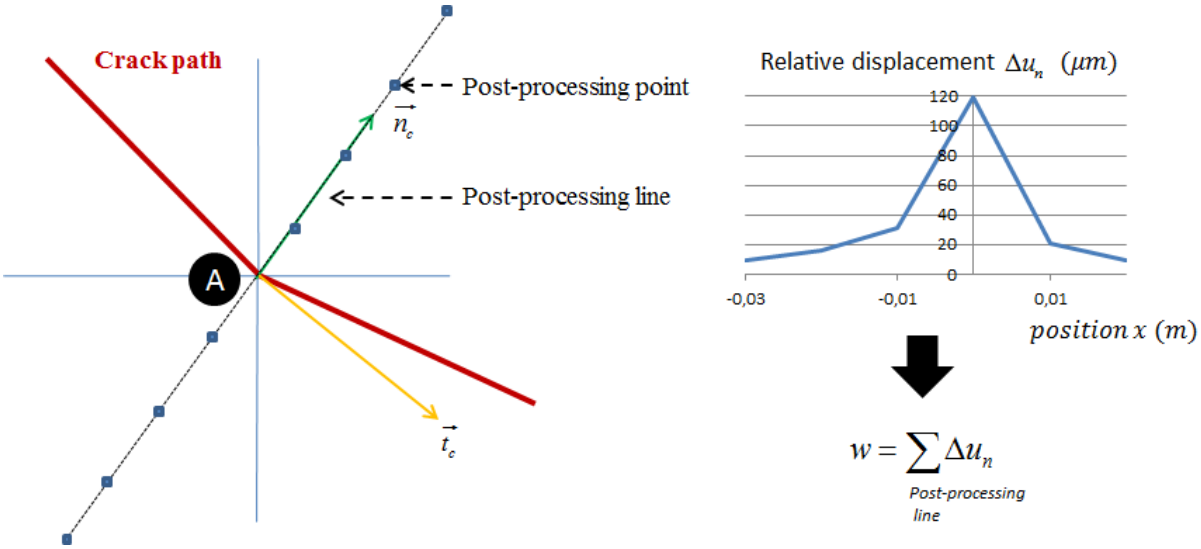

Figure 19. Computation of the normal crack opening.

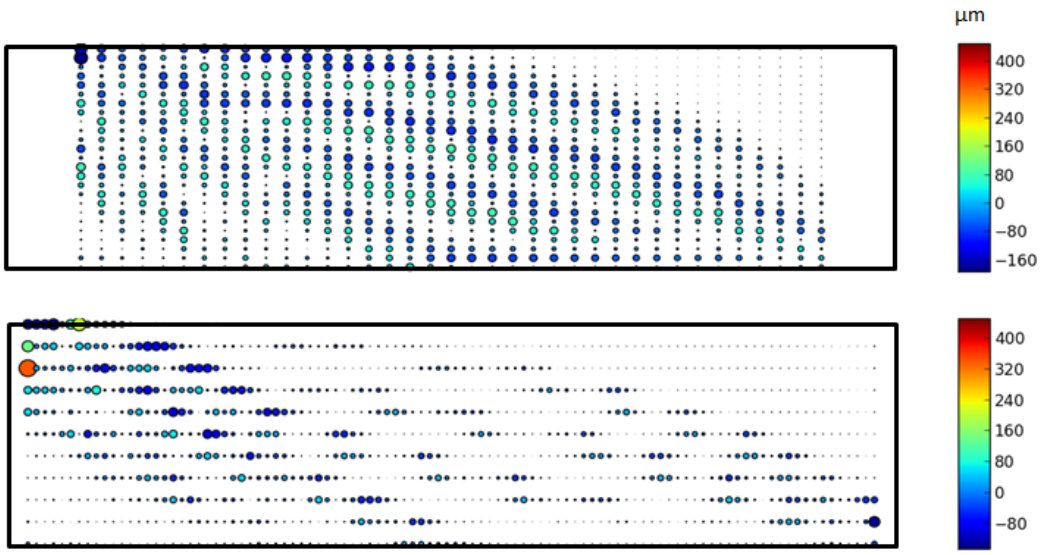

Figure 20. Distribution of the bond slip at a force of 3900 kN, along vertical reinforcement (top) and horizontal reinforcement (bottom)

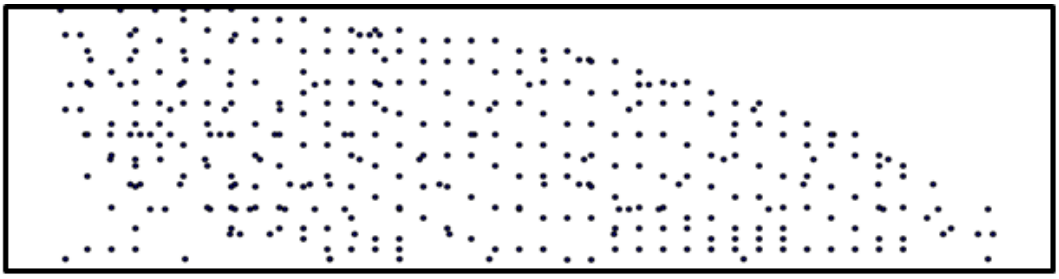

Figure 21. Crack positions calculated from the change in the slip sign

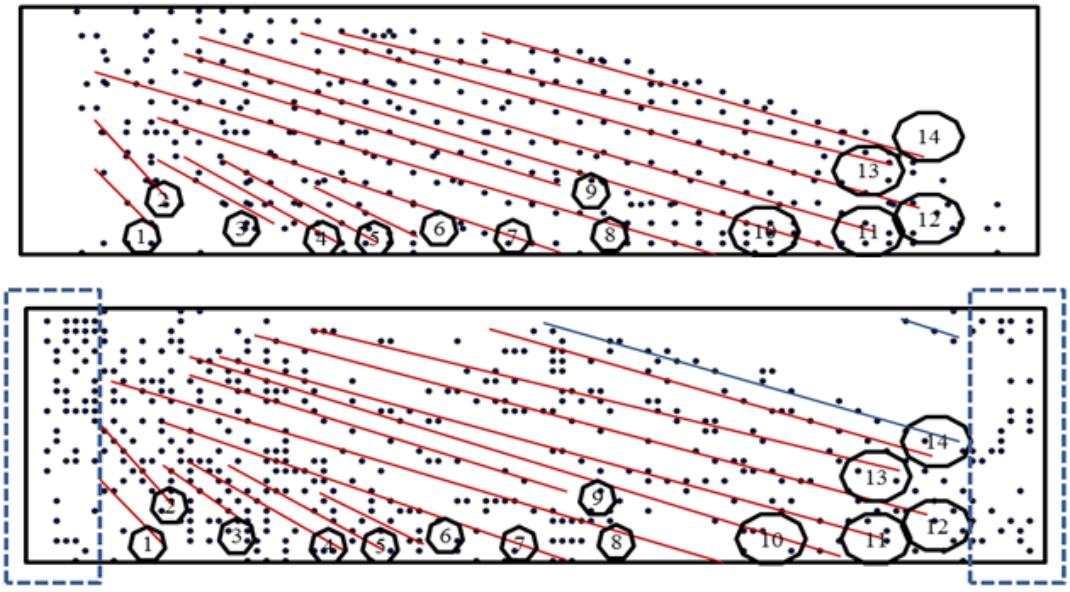

Figure 22. Comparison between the methods based on the slip (top) and on the relative displacement (bottom) to determine the crack pattern on the external face at a force of 3900 kN. Straight red lines correspond to cracks in common, blue lines correspond to differences in the crack pattern

The comparison between the two simulated crack paths (from slip and from displacement steps) is shown in Figure 22. The mains cracks are similar in both cases, which tends to confirm the hypothesis of crossing cracks which appear both on surface and at the position of the steel bars. The differences (blue lines and blue dashed boxes in Figure 22) only concern secondary cracks which are less of interest in our proposed comparison.

In addition to Figure 22, Figure 23 illustrates the simulated crack path in the zone of interest. It is on this zone that the crack properties are experimentally determined using the digital image correlation [30]. The order of apparition of the cracks is first compared (Figure 24). Cracks initiate on the loaded side. At a force of 2100 kN, a new crack appears on the opposite side. Finally, the cracks propagate once again from the loaded side. This phenomenon is quite well reproduced by the simulation. Compared to the damage distributions (Figure 12), the proposed method enables to better localize the mechanical degradation.

From the crack path, it is possible to compute the average spacing and crack angle in the zone of interest. The comparison between experiment and simulation is provided in Table 4 for a force of 3900 kN. A good agreement is once again obtained.

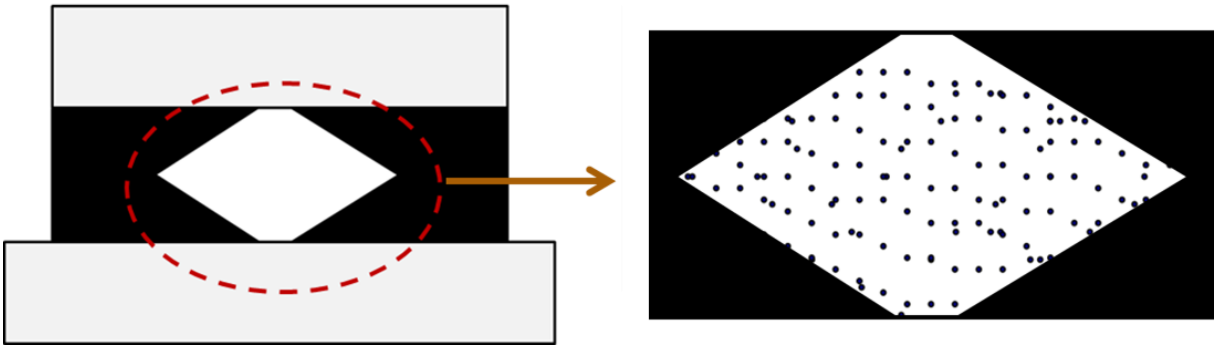

Figure 23. Simulated crack pattern at a force of 3900 kN in the zone of interest.

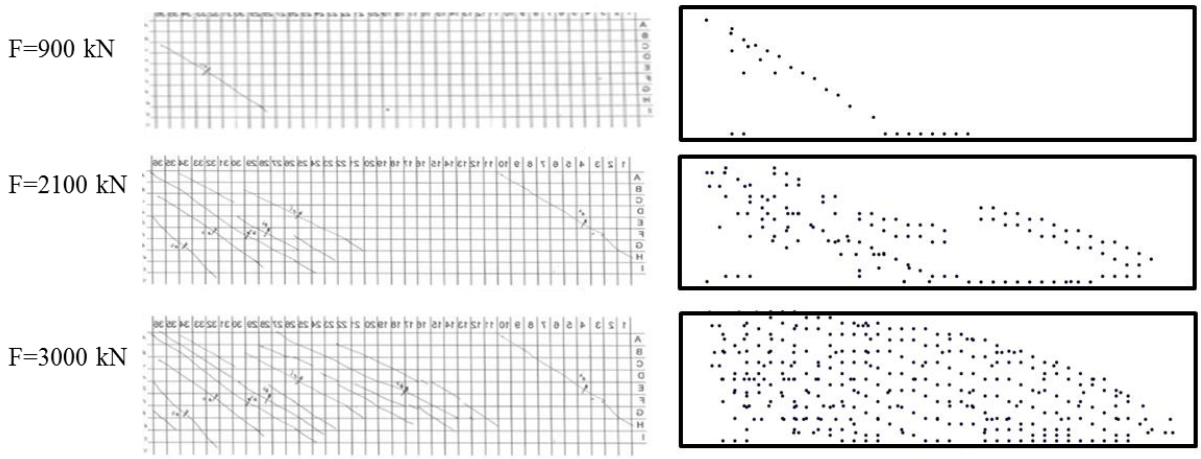

Figure 24. Order of crack apparition. Experiment (left) and simulation (right)

F = 3900 kN	Mean crack angle	Mean crack spacing
	θ_c (degree)	(mm)
Experiment	28.5	97.4
Simulation	25	98

Table 4. Crack spacing and angle

5.2 Crack opening

From the crack path, the normal crack opening can be computed using the methodology described in the previous section. The distribution of the normal crack opening in the zone of interest is provided in Figure 25. From this result, it is possible to compute the mean and the maximum crack openings. The comparison with the experiment is shown in Table 5. A good agreement is obtained. It is to be noted that these results only reflect one simulation with one set of parameters. To be improved, a statistical study should be performed in order to evaluate the effect of uncertainties on input parameters (geometrical or material parameters especially). Nevertheless, even if not performed, this contribution shows that without any particular effort on the calibration of the model parameters, it is possible to obtain, with the proposed steel – concrete bond model, a good agreement, even on local properties like crack opening. The nature of the agreement (difference of 2 microns between experiment and simulation) is here obviously qualitative, especially for concrete structures for which the reproducibility of the test results at such a scale can be questioned (only one experiment was performed in the considered experimental campaign).

With this new post-processing method, further cracking mechanisms can also be investigated. Normal and tangential crack openings can especially be distinguished. For example, Figure 26 illustrates the evolution of the normal and tangential crack openings for the point with the maximum normal crack opening. For a displacement less than 0.75 mm, normal and tangential crack openings are nearly identical. Normal opening then increases significantly compared to the tangential one, up to an imposed displacement equal to 1.5 mm. At this point, the normal crack opening is approximately 3 times larger than the tangential one. Figure 27 illustrates the distributions of the normal and tangential crack openings for a force equal to 3900 kN. It shows that the tangential opening is significant even at the end of the computation (Table 6).

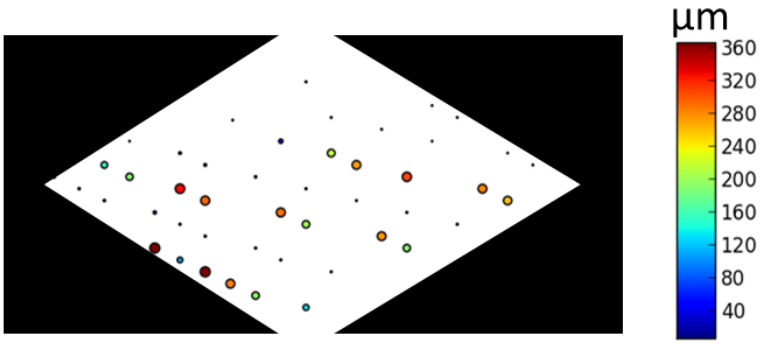

Figure 25. Distribution of the normal crack opening (F = 3900 kN)

F = 3900 kN	Mean crack opening (µm)	Maximum crack opening (µm)
Experiment	105	364
Simulation	109	366

Table 5. Crack opening. Comparison between simulation and experiment

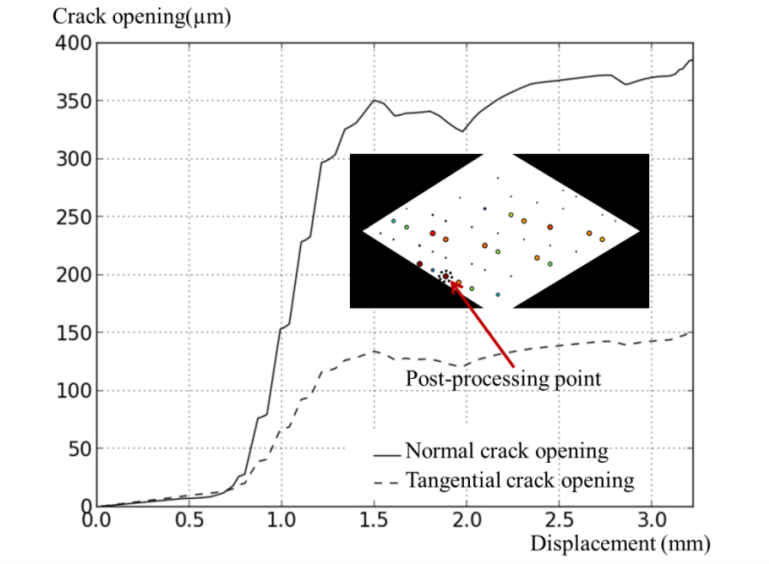

Figure 26. Evolution of crack opening in the normal direction and in the tangential direction

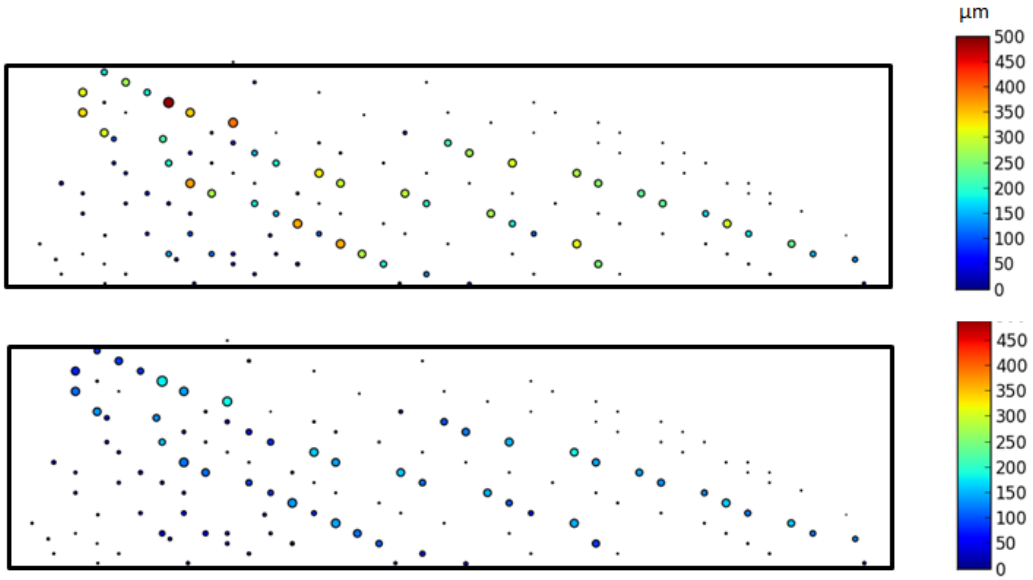

Figure 27. Normal crack opening (top) and tangential crack opening (bottom) using the new post-processing method for a force equal to 3900 kN (external face)

Finally, it is to be noted that the proposed method uses the "total" relative displacements. It implies that both elastic and inelastic part of the behavior is taken into account in the calculation of the crack openings. On the contrary, in [29] for example, a decomposition between the "cracking" (or inelastic) and elastic strains is added. Only the cracking strain is then used to calculate the crack properties. To investigate this point, the so-called cracking and elastic strains are computed on the shear wall using the method proposed in [29] and implemented in the finite element code Cast3M [23]. Resulting crack openings are compared to "elastic" openings by multiplying the cracking strain (or elastic strain respectively) by a length related to the mean element size (see [29] for details) (Figure 28). These results show that once the crack is localized, the "elastic opening" (Figure 28 top) becomes negligible compared to the cracking one (Figure 28 bottom). In this case, the decomposition between the elastic and inelastic behaviors does not seem necessary and thus validates the principle of our approach.

F = 3900 kN	Normal crack opening (µm)	Tangential crack opening (µm)
Maximum crack opening	488	186
Mean crack opening	102	60

Table 6. Calculated crack opening. Comparison between normal and tangential crack openings for a force equal to 3900 kN (external face)

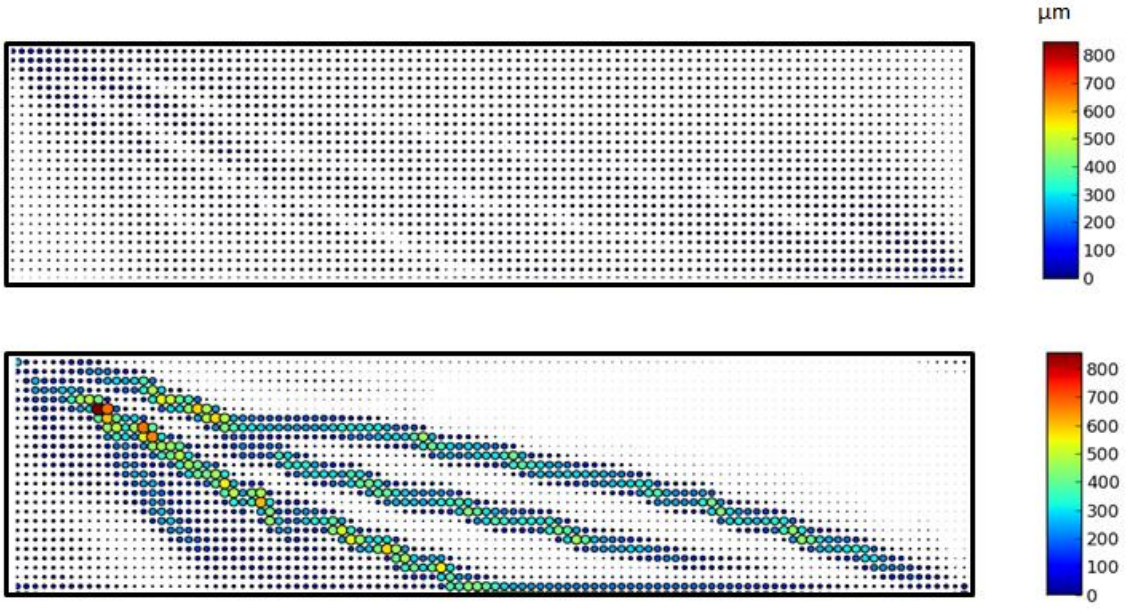

Figure 28. Crack opening (bottom) and "elastic" opening (top) following [29]

5.3 Discussion on the influence of the steel – concrete bond

In this part, the interest of including the proposed bond model is discussed compared to a more classical no-slip "perfect" relation. To this aim, a second computation is performed. Each steel node has the same displacement as the concrete element in which it is included (zero slip). This so-called "perfect" bond is applied using additional kinematic relations.

Figure 29 gives the comparison between the two simulations in terms of force – displacement curve. The same evolution is globally obtained and no significant difference can be noticed. The elastic zone is the same, due to the high value of the initial slope in the bond stress-bond slip curve.

Figure 30 illustrates the comparison for the crack pattern at the ultimate load using the distribution of the norm of the relative displacement in the horizontal directions. The post-processing method based on the slip cannot be used here (no slip when the perfect relation hypothesis is used). So the alternative method based on the displacements step is required. Localization near the loaded zone is observed with the perfect elation. It was expected since this hypothesis stiffens the bond between steel and concrete and may induce heavy damage on concrete (shear stress especially). This difference may have a great impact, especially when questions about dimensioning are considered. Larger crack openings may indeed induce additional reinforcement in the structure and trigger larger industrial costs.

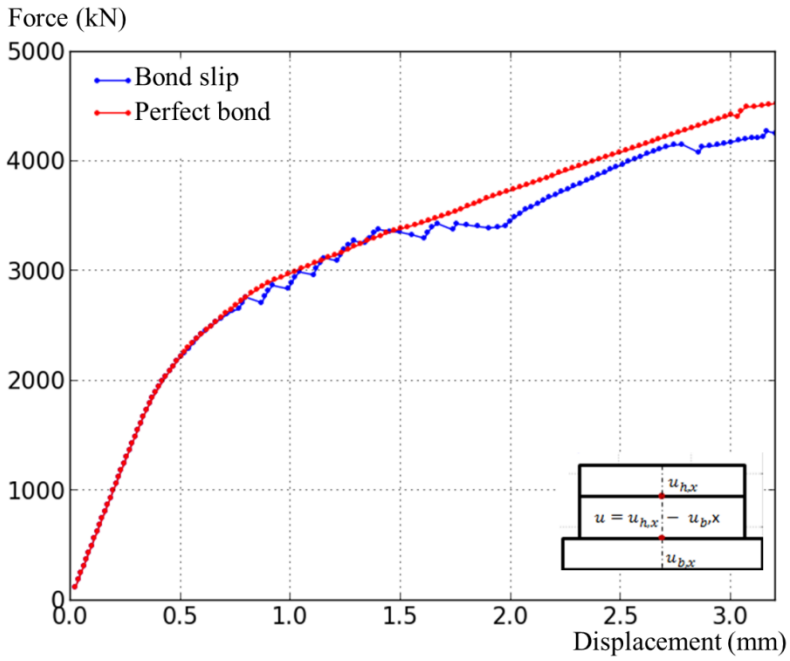

Figure 29. Comparison between the perfect relation and the bond slip model for the force-displacement curve

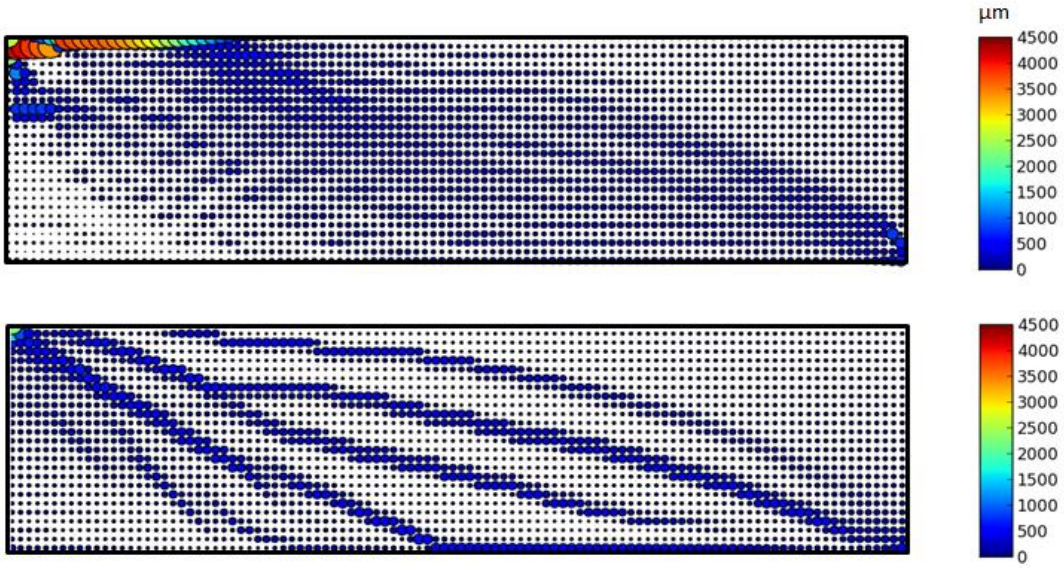

Figure 30. Comparison of the crack patterns at the ultimate load considering the perfect relation (top) and the bond model (bottom)(norm of the relative displacements)

Finally, Figure 31 illustrates the norm of the relative displacements in the interest zone for both simulations. The distribution is quasi-uniform when using the perfect bond (homogenization effect). On the contrary, with the bond model, cracks are more localized and more representative

These differences, associated with the proposed experimental comparison using the bond model, underline the interest of including a representative bond model in the simulation if local values (crack openings for example) want to be achieved.

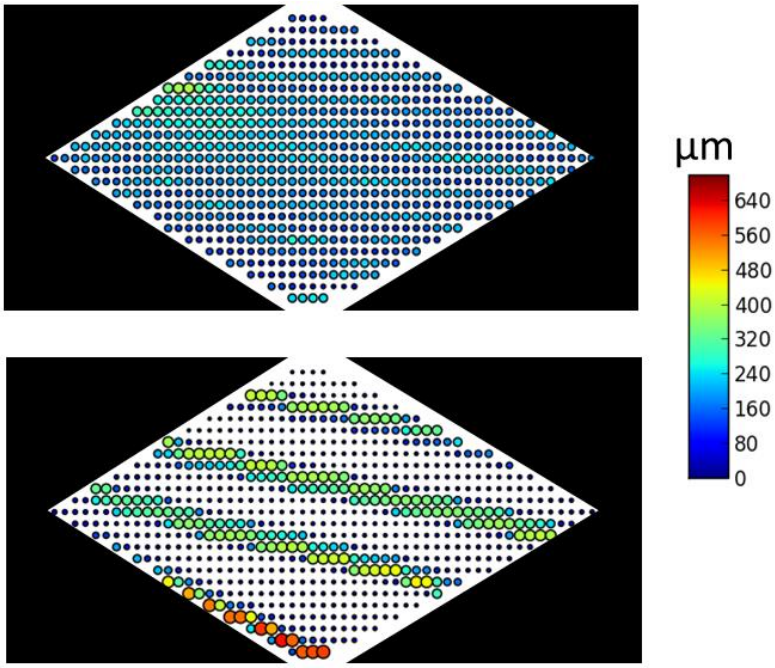

Figure 31. Comparison of the crack patterns) at the ultimate load in the interest zone considering the perfect relation (top) and the bond slip model (bottom) (norm of the relative displacements)

6 Conclusions

A new steel-concrete bond model was applied to a reinforced concrete shear wall. The bond model, adapted for industrial computations, is based on an interface element which relates 1D steel bars with 3D surrounding concrete. The global structural behavior was correctly captured.

Due to a complex crack pattern (oriented cracks especially and variable crack angles), a new post-processing method to compute crack properties from a damage model was also proposed. It takes advantage of the calculation of the slip between steel and concrete and relates the crack position to the change in the sign of the slip. The crack opening is then computed from the relative displacement in the normal direction of the crack. The method is applicable independently on the chosen concrete damage models and for 3D applications (reconstruction of the crack surface from the crack lines in each cross section). Nevertheless, as the exact position of the cracks is computed at the reinforcement location, crossing cracks have to be assumed, which is typically the case for classical applications (bending beams, shear wall …). Compared to more classical methods which detect the crack from the nodal displacements, this method is of more direct application and does not suppose any additional hypothesis like crack apparition criterion or a priori crack direction. The method is quasi-automatic but still requires a correct methodology for the automatic determination of the crack path (search direction for example).

The methodology was successfully applied on the simulation of a reinforced concrete shear wall. The comparison with the experimental results (digital image correlation) provided a good agreement and validated the application of the proposed method to reinforced concrete structures, even in a case of a complex crack pattern.

Finally, the role of the steel concrete bond model was discussed, compared to a more classical perfect (no-slip) relation for whom the same displacements between steel and concrete are assumed. No clear difference appears in the global behavior (force – displacement curve).

Concerning the crack distribution, the perfect relation leads to a heavier mechanical degradation near the loading point and a more regularized distribution in the current part, which is less in agreement with experiment.

References

[1] Eurocode 2. Calcul des Structures en béton, NF-EN-1992 (2007)

[2] M.A. Polak, F.J. Vecchio, Nonlinear analysis of reinforced concrete shells, Journal of Structural Engineering 119 (12) (1993) 3439-3462

[3] A. Hillerborg, M. Modeeer, P.E. Peterson, Analysis of crack formation and crack growth in concrete by means of fracture mechanics and finite elements, Cement and Concrete Research 6 (6) (1976) 773-782

[4] H.D. Bui, Mécanique de la rupture fragile. Masson, Paris (1978)

[5] G.I. Barenblatt, The mathematical theory of equilibrium cracks in brittle fracture, Advanced Applied Mechanics 7 (1962) 55–129

[6] J. Lemaitre, J.L. Chaboche, Aspect phénoménologique de la rupture par endommagement, Journal de Mécanique Appliquée 2 (1978) 317-365

[7] R. Faria, J. Oliver, M. Cervera, A strain based plastic viscous-damage model for massive concrete structures, International Journal of Solids and Structures 35 (14) (1998), 1533-1558

[8] L. Jason, A. Huerta, G. Pijaudier-Cabot, S. Ghavamian, An elastic plastic damage formulation for concrete. Application to elementary tests and comparison with an isotropic damage model, Computational Methods in Applied Mechanics and Engineering 195 (52) (2006), 7077-7092

[9] J. Mazars, Application de la mécanique de l'endommagement au comportement non linéaire et à la rupture du béton de structure, PhD Thesis, Université Pierre et Marie Curie (1984)

[10] S. Fichant, C. La Borderie, G. Pijaudier-Cabot, Isotropic and anisotropic descriptions of damage in concrete structures, Mechanics of Cohesive Frictional Materials 4 (1999) 339-359

[11] L. Jason, A. Torre-Casanova, L. Davenne, X. Pinelli, Cracking behavior of reinforced concrete beams. Experiment and simulations on the numerical influence of the steel concrete bond, International Journal of Fracture 180 (2) (2013), 243-250

[12] D. Ngo, A.C. Scordelis, Finite element analysis of reinforced concrete beams, ACI Journal 64 (1967), 152-163

[13] D. Brancherie, A. Ibrahimbegovic, Novel anisotropic continuum-discrete model capable of representing localized failure of massive structures. Part I: Theoretical formulation and numerical implementation, Engineering Computations 26 (2009) 100-127

[14] N. Dominguez, D. Brancherie, L. Davenne, A. Ibrahimbegovic, Prediction of crack pattern distribution in reinforced concrete by coupling a strong discontinuity model of concrete cracking and a bond slip of reinforcement model, Engineering Computations 22 (2005) 558-582

[15] N. Dominguez, Etude de la liaison-acier enter l'acier et le béton: de la modélisation du phénomène à la formulation d'un élément enrichi "Béton Armé", PhD thesis, Ecole Normale Supérieure de Cachan (2005)

[16] A. Ibrahimbegovic, A. Boulkertous, L. Davenne, D. Brancherie, Modeling of reinforced concrete structures providing crack spacing based on XFEM, EDFEM and novel operator split solution procedure, International Journal of Numerical Methods in Engineering 83 (2010) 452-481

[17] A. Casanova, L. Jason, L. Davenne, Bond slip model for the simulation of reinforced concrete structures, Engineering Structures 39 (2012) 66-78

[18] C. Mang, L. Jason, L. Davenne, A new bond slip model for reinforced concrete structures in monotonic and cyclic loadings, Engineering Computations 32 (7) (2015)

[19] A. Torre-Casanova, L. Jason, L. Davenne, X. Pinelli, Confinement effects on the steel-concrete bond strength and pull-out failure, Engineering Fracture Mechanics 97 (2013) 92-104

[20] CEOS.FR French National Project, www.ceosfr.org (2015)

[21] G. Ruocci, D. Chebl, S. Erlicher, P. Bisch, Experimental Investigation and engineering interpretation on shear cracking in RC walls due to cyclic loading, Proceeding of SMIRT 2013 conference (2013)

[22] B. Belletti, R. Esposito, C. Damoni, Numerical prediction of the response of a squat shear wall subjected to monotonic loading through PARC_CL model, Proceeding of the VIII International Conference on Fracture Mechanics of Concrete and Concrete Structures (FraMCoS-8) (2013)

[23] Cast3M, www-cast3m.cea.fr (2015)

[24] C. Comi, S. Mariani, U. Perego, An extended FE strategy for transition from continuum damage to mode I cohesive crack propagation, International Journal for Numerical and Analytical Methods in Geomechanics 31 (2) (2007) 213-238

[25] A. Simone, G.N. Wells, L.J. Sluys, From continuous to discontinuous failure in a gradient enhanced continuum damage model, Computer Methods in Applied Mechanics and Engineering 192 (2003) 4581-4607

[26] J. Mazars, G. Pijaudier-Cabot, From damage to fracture mechanics and conversely: a combined approach, International Journal of Solids and Structures 33 (1996) 3327-3342

[27] J. Oliver, A.E. Huespe, M.D.G. Pulido, E. Chaves, From continuum mechanics to fracture mechanics: the strong discontinuity approach, Engineering Fracture Mechanics 69 (2002) 113-136

[28] F. Dufour, G. Pijaudier-Cabot, M. Choinska, A. Huerta, Extraction of a crack opening from a continuous approach using regularized damage models, Computers and concrete 5 (4) (2008) 375-388

[29] M. Matallah, C. La Borderie, O. Maurel, A practical method to estimate crack opening in concrete structures, International Journal of Numerical and Analytical Methods in Geomechanics 34 (2010) 1615–1633

[30] G. Ruocci, C. Rospars, P. Bisch, S. Erlicher, G. Moreau, Cracks distance width in reinforced concrete membranes: experimental results from cyclic loading histories, Proceedings of the 15th WCCE conference, Lisboa, Portugal (2012)

[31] J. Rethoré, F. Hild, S. Roux, Extended digital image correlation with crack shape optimization, International journal for numerical methods in engineering 73 (2007) 248-272

[32] T. Wang, T.C. Hutchinson, Gas leakage rate through reinforced concrete shearwall: numerical study, Nuclear Engineering and Design 235 (2005) 2246-2260

[33] G. Pijaudier-Cabot, Z.P. Bazant, Nonlocal damage theory, Journal of Engineering Mechanics 113 (1987) 1512-1533